ARTICLE

BIOTECHNOLOGY and BIOENGINEERING

Assessment of Nitric Oxide (NO) Redox Reactions Contribution to Nitrous Oxide (N_2O) Formation During Nitrification Using a Multispecies Metabolic Network Model

Octavio Perez-Garcia,[1] Kartik Chandran,[2] Silas G. Villas-Boas,[3] Naresh Singhal[1]

[1]Department of Civil and Environmental Engineering, University of Auckland, 20 Symonds Street, Auckland, New Zealand; telephone: +64-9-923 4512; fax: +64-9-373 7462; e-mail: octavio.perez@auckland.ac.nz; e-mail: n.singhal@auckland.ac.nz

[2]Department of Earth and Environmental Engineering, Columbia University, New York, New York

[3]School of Biological Sciences, University of Auckland, Auckland, New Zealand

ABSTRACT: Over the coming decades nitrous oxide (N_2O) is expected to become a dominant greenhouse gas and atmospheric ozone depleting substance. In wastewater treatment systems, N_2O is majorly produced by nitrifying microbes through biochemical reduction of nitrite (NO_2^-) and nitric oxide (NO). However it is unknown if the amount of N_2O formed is affected by alternative NO redox reactions catalyzed by oxidative nitrite oxidoreductase (NirK), cytochromes (i.e., P460 [Cyt_{P460}] and 554 [Cyt_{554}]) and flavohemoglobins (Hmp) in ammonia- and nitrite-oxidizing bacteria (AOB and NOB, respectively). In this study, a mathematical model is developed to assess how N_2O formation is affected by such alternative nitrogen redox transformations. The developed multispecies metabolic network model captures the nitrogen respiratory pathways inferred from genomes of eight AOB and NOB species. The performance of model variants, obtained as different combinations of active NO redox reactions, was assessed against nine experimental datasets for nitrifying cultures producing N_2O at different concentration of electron donor and acceptor. Model predicted metabolic fluxes show that only variants that included NO oxidation to NO_2^- by Cyt_{P460} and Hmp in AOB gave statistically similar estimates to observed production rates of N_2O, NO, NO_2^- and nitrate (NO_3^-), together with fractions of AOB and NOB species in biomass. Simulations showed that NO oxidation to NO_2^- decreased N_2O formation by 60% without changing culture's NO_2^- production rate. Model variants including NO reduction to N_2O by Cyt_{554} and cNor in NOB did not improve the accuracy of experimental datasets estimates, suggesting null N_2O production by NOB during nitrification. Finally, the analysis shows that in nitrifying cultures transitioning from dissolved oxygen levels above 3.8 ± 0.38 to $<1.5 \pm 0.8$ mg/L, NOB cells can oxidize the NO produced by AOB through reactions catalyzed by oxidative NirK.

Biotechnol. Bioeng. 2016;113: 1124–1136.

KEYWORDS: metabolic modeling; nitrous oxide emission; nitrification; oxidreductase enzymes; AOB; NOB

Introduction

Nitrous oxide (N_2O), a potent atmospheric greenhouse gas and ozone depleting substance, can be emitted from wastewater treatment plants (WWTP) (Ahn et al., 2010; Foley et al., 2010; Kampschreur et al., 2009). Even though N_2O emissions from WWTPs are generally reported to be lower than those from agricultural soils and manure management systems (Wuebbles, 2009), they are acknowledged by water utilities as significant contributors to the carbon footprint of WWTPs as carbon dioxide equivalent emission (Ni et al., 2013; Wang et al., 2011). Such N_2O emissions generally range between 0.01 and 2% of influent nitrogen load, but variations in the concentrations of oxygen, nitrite, and ammonia in wastewater can magnify N_2O emissions to as much as 25% of the influent nitrogen load (Kampschreur et al., 2008, 2009). However, the mode of how such variations influence N_2O formation has to be defined clearly in order to formulate operational strategies that limit N_2O emissions from WWTP.

Ammonia-oxidizing bacteria (AOB) are major contributors to N_2O production during biological nitrification (Kampschreur et al., 2007; Yu et al., 2010). N_2O production by AOB occurs via two pathways: (i) hydroxylamine oxidoreductase (HAO) mediation and (ii) the nitrite reductase (NirK) mediation (a.k.a. nitrifier denitrification) (Kampschreur et al., 2009; Schreiber et al., 2012;

Correspondence to: N. Singhal and O. Perez-Garcia
Contract grant sponsor: University of Auckland
Contract grant sponsor: Mexican National Council for Science and Technology (CONACyT)
Received 12 July 2015; Revision received 29 September 2015; Accepted 1 November 2015
Accepted manuscript online 19 October 2015;
Article first published online 26 November 2015 in Wiley Online Library (http://onlinelibrary.wiley.com/doi/10.1002/bit.25880/abstract).
DOI 10.1002/bit.25880

Stein, 2010; Yu et al., 2010). Both pathways involve an initial formation of nitric oxide (NO) by HAO or NirK, followed by reduction to N_2O by nitric oxide reductase (cNor) (Stein, 2010). NO is therefore the precursor and plays a critical role in N_2O formation. NirK, HAO, and cNor are not the only enzymes catalyzing NO production or consumption in nitrifying cultures; Cytochromes, flavohemoglobins and nitrite oxidoreductases can also catalyze NO redox reactions (Schreiber et al., 2012; Stein, 2010; Whittaker et al., 2000). To accommodate such uncertainties mechanistic mathematical models for N_2O formation during nitrification resort to using "artificial" parameters, such as anoxic correction factor, η_{AOB}, to fit experimental data (Law et al., 2012; Ni et al., 2013).

Of the biological redox reactions forming or dissipating NO (Fig. 1) enzymes involvement in the following reactions is poorly understood: (i) NO oxidation to NO_2^- in AOB; (ii) NO oxidation to NO_2^- in nitrite-oxidizing bacteria (NOB); and (iii) NO reduction to N_2O in NOB. The significance of reactions (i) and (ii) is that the genomes of AOB (e.g., *Nitrosomonas europaea*, *Nitrosomonas eutropha*, and *Nitrosococcus oceani*) and NOB (e.g., *Nitrospira defluvii*, *Nitrobacter winogradskyi*, and *Nitrobacter hamburgensis*) indicate that they can synthesize Cytochrome P460 (Cyt_{P460}), flavohemoglobins (Hmp) and nitrite oxidoreductase (NirK), known to oxidize NO to NO_2^- (Chain et al., 2003; Lücker et al., 2010; Schreiber et al., 2012; Starkenburg et al., 2011; Stein, 2010, 2011; Whittaker et al., 2000). Cyt_{P460} obtained from *N. europaea* cultures have been shown to oxidize NO and NH_2OH to NO_2^- and the gene sequence for producing Cyt_{P460} is widespread in the genomes of AOB (Elmore et al., 2007; Numata et al., 1990). Similarly, Hmp, widely distributed among AOB, NOB, and heterotrophic denitrifying bacteria, functions as NO dioxygenase or reductase during nitrosative stress (Stein, 2010). In addition to AOB mediated pathways, the genomes of NOB such as *Nitrospina gracilis* and *Nitrobacter hamburgensis* suggest that they can form N_2O via NO reduction reactions catalyzed by cytochrome c554 (Cyt_{c554}) and cNor (Lücker et al., 2013; Starkenburg et al., 2008a). This indicates the potential for another route for N_2O formation besides the two AOB mediated pathways. The expression of Cyt_{P460}, Hmp and oxidative NirK genes has however not been reported in nitrifying cultures producing N_2O.

The putative contribution of alternative NO redox reactions on N_2O formation in nitrification has not been investigated experimentally. Neither modeling studies had evaluated the role of such reactions by analyzing experimental data (Mampaey et al., 2013). Assessing such contributions by experimentally measuring the rates of metabolic redox reactions in AOB and NOB is complicated by the dynamic nature and small spatial scale of NO and N_2O formation (Schreiber et al., 2012). An alternative approach is to mathematically quantify the rates of all the metabolic reactions involved in nitrogen transformation using approaches such as flux balance analysis (FBA) of stoichiometric metabolic network (SMN) models (Orth et al., 2010; Perez-Garcia et al., 2014b; Varma and Palsson, 1994a). SMN models have generally been applied to model the metabolism of single species; however, the technique can be adapted to model multispecies systems (Chaganti et al., 2011; Dias et al., 2005; Pardelha et al., 2012; Stolyar et al., 2007). In this study

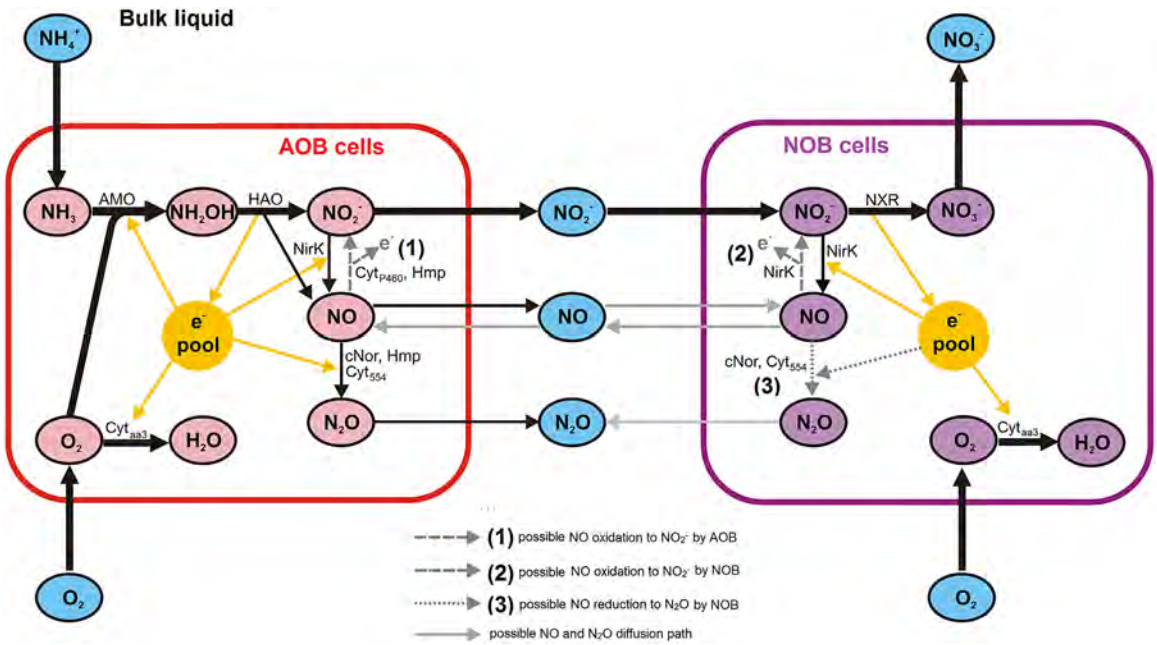

Figure 1. Scheme illustrating the routes for production and consumption of NO and N_2O in nitrifying microbial communities. The contributions of reactions for NO oxidation to NO_2^- and reduction to N_2O by NOBs on the net amount of NO and N_2O formed in nitrifying mixed cultures is not known. Nodes represent chemical compounds; thick arrows represent the main route of ammonium (NH_4^+) oxidation to nitrite (NO_2^-) by AOBs and from NO_2^- to nitrate (NO_3^-) by NOB; yellow arrows represent routes of electron flow from or toward nitrogen redox reactions. Encoded enzymes in AOB and NOB genomes are depicted as follow: AMO, ammonia monooxygenase (genes *amoABC*); HAO, hydroxylamine oxidoreductase (genes *haoAB*); NXR, nitrite oxidoreductase (gene *nxrA-K*); NirK, cooper-containing nitrite reductase (gene *nirK*); Cyt_{P460}, Cytochrome P460 (gene *cyp*); Cyt_{aa3}, terminal oxidase cytochrome aa3 (genes *cox*); cNor, nitric oxide reductase (genes *norABC*); Cyt_{554}, cytochrome c554 (gene *cyc*); Hmp, flavohemoglobins (gene *hmp*).

we extend our earlier SMN model for *Nitrosomonas europaea* (Perez-Garcia et al., 2014b) to a multispecies metabolic network. This allows us to capture the large diversity of redox reactions involving transformations of inorganic nitrogenous compounds within nitrifying microbial communities. The objective of this study is to evaluate the effect of alternative NO redox reactions on N_2O production and microbial metabolism of nitrifying mixed cultures operated at different concentration of electron donor (NH_4^+, NH_2OH [hydroxylamine], and NO_2^-) and acceptors (O_2 and NO_2^-) using the developed multispecies SMN model. Even though, at its current state, the presented model do not predicts variations of nitrogenous compounds across time, it provides great details fine biochemical and ecological mechanisms involved in nitrogen transformations during nitrification.

Materials and Methods

Nitrifying Cultures Analyzed

The model was used to analyze nine datasets (referred to as A to I) from previously reported experimental findings for nitrifying cultures (Ahn et al., 2011; Law et al., 2012; Wunderlin et al., 2013). These experiments involved one of the following nitrification processes: (i) ammonium oxidation to nitrate by AOB and NOB, (ii) ammonium oxidation to nitrite by AOB, (iii) nitrite oxidation to nitrate by NOB, or (iv) hydroxylamine oxidation to nitrite and nitrate (NOx) by AOB and NOB. The experimental conditions for these experiments are summarized in Table I, and include specifications for the initial concentrations of electron donors and acceptors, the specific oxygen and ammonium uptake rates (respectively, sOUR and sAUR), and the specific N_2O production rate (sN_2OPR) corresponding to maximum observed N_2O productivity. Additionally, Table II lists the fraction of total biomass for the most abundant AOB and NOB species. The means and standard deviations of 38 variables characterizing the cellular metabolism of AOB and NOB populations at the moment of maximum N_2O production productivity (Table SI of *supporting information* [*SI*]) were obtained as specified in section S1 and S2 of *SI*, using the reported concentrations of substrates and products, along with the bioreactor operation conditions.

SMN Model Development

The multispecies stoichiometric metabolic network (SMN) model was developed for four AOB (*Nitrosomonas europaea*, *Nitrosomonas eutropha*, *Nitrosospira multiformis*, and *Nitrosococcus oceani*) and four NOB (*Candidatus* Nitrospira defluvii, *Nitrobacter winogradskyi*, *Nitrobacter hamburgensis*, and *Nitrospina gracilis*) species. These species were selected for availability of genomic data and abundance in nitrifying cultures investigated, and covered the variety of nitrogen related respiratory redox reactions occurring in the nitrifying microbial communities of the cultures.

A SMN for each species was constructed by following the procedure outlined in Thiele and Palsson (2010) and using organism-specific genomic and biochemical information obtained from literature and online biochemical databases KEGG (http://www.genome.jp/kegg/), NCBI (http://www.ncbi.nlm.nih.gov/), and MetaCyc (http://metacyc.org/). Each network consisted of a list of metabolites and equations for biochemical reactions for: (i) respiration of inorganic nitrogenous compounds (specified in Table III); (ii) electron transport chain, including ATP and NADH synthesis; and (iii) production of protein and biomass using ATP and NADH. Each equation was elementally and charge balanced, thermodynamically classified as reversible or irreversible, and modeled to occur in the extracellular, periplasmic, or cytoplasmic cell sub-compartments (Savinell and Palsson, 1992; Thiele and Palsson, 2010).

A multi-compartment approach was used to develop the multispecies SMN (Klitgord and Segrè, 2010; Stolyar et al., 2007; Taffs et al., 2009) in which the SMN for each species were assigned to individual compartments within the same metabolic network. A ninth compartment was added to represent the microbes' common environment, through which certain compounds can be transferred between the eight organisms (e.g., NO_2^- and NO). Then, transport equations were added for metabolites that could be taken up by, or secreted from, each species (Figure 2A). Note that the same compunds in different compartment are treated as different metabolites connected by transport fluxes (Stolyar et al., 2007). Consequently, the amount of metabolite pooled on the common environment equals the sum of metabolite produced and consumed by the eight species. Such common metabolites are inorganic nitrogenous compounds (NH_4^+, NH_2OH, NO_3^-, NO_2^-, NO, N_2O, and N_2), oxygen (O_2), orthophosphate (PO_4^{-3}), carbon dioxide (CO_2), protons (H_2), and water (H_2O). Finally, exchange equations were added the common environment compartment to represent net uptake or secretion of substrates and products for the whole microbial community. Rates (fluxes) of exchange equations were either set equal to zero (indicating no net production or depletion), set to the experimental measurement, or allowed to be flexible. The particular conditions for each simulation are described in the folowing sections.

The complete multispecies SMN model contains 407 reactions involving 380 metabolic compounds distributed across 25 compartments/sub-compartments (three cell sub-compartments in each of the eight species compartments plus one common environment compartment). The complete model can be found on the Table SV of *SI*. Figure 2B shows a visualization of the participating metabolites and reactions, with nodes representing both reactions and metabolites. Nodes of species-specific SMNs form eight clusters around the nodes representing substrate and product compounds pooled on the common environment. The figure shows the number of reactions and metabolites of the eight species-specific SMNs and specifies all the substrates and products (labelled nodes at the periphery of network) modelled for the whole microbial community.

Flux Balance Analysis

Model simulations were performed in Matlab®7 R2013b (MathWorks Inc., Natick, MA) using the FBA algorithm of the COBRA toolbox 2.0 (Schellenberger et al., 2011) with the linear programming solver GLPK (GNU project, Moscow, Russia). In the FBA simulations the microbial community metabolic network was mathematically represented as an $m \times n$ stoichiometric matrix, $S(m \times n)$, containing m metabolites participating in n reactions. The matrix element $s_{i,j}$ represents the stoichiometric

Table I. Published experimental datasets simulated using the multispecies SMN developed in this study. Details of the experimental conditions can be found in the section S1 of SI. The terms DO, sOUR, sAUR, and sN_2OPR refer to dissolved oxygen concentration and observed specific rates of oxygen uptake, ammonium uptake, and N_2O production. All rates expressions were normalized for the amount of biomass in cultures expressed as chemical oxygen demand (COD, assuming 1 g of dry biomass corresponds to 1.42 g of COD (Grady et al., 1999)).

				Specific rates at the moment of maximum N_2O productivity. Mean ± Std. dev.		
Process	Experiment ID	Publication	Experiment's initial concentrations of electron donor and acceptor	sOUR ($mmol\text{-}O_2\ gCOD^{-1}\ h^{-1}$)	sAUR ($mmol\text{-}N\ gCOD^{-1}\ h^{-1}$)	sN_2OPR ($mmol\text{-}N\ gCOD^{-1}\ h^{-1}$)
Ammonium oxidation to nitrate by AOB and NOB 	A	Ahn et al. (2011)	DO = 3.8 ± 0.38 mg-O_2/L Influent NH_4^+ = 500 mg-N/L	2.82 ± 0.35	2.44 ± 0.81	0.004 ± 0.0028
	B	Ahn et al. (2011)	DO = 1.5 ± 0.87 mg-O_2/L Influent NH_4^+ = 500 mg-N/L	2.81 ± 0.32	1.44 ± 0.11	0.071 ± 0.025
	C	Wunderlin et al. (2012, 2013)	DO = 1.9 ± 0.2 mg-O_2/L Initial NH_4^+ = 2.5 mg-N/L	0.26 ± 0.003	0.1 ± 0.01	0.002 ± 0.002
Ammonium oxidation to nitrite by AOB 	D	Ahn et al. (2011)	DO = 1.1 ± 0.38 mg-O_2/L Influent NH_4^+ = 500 mg-N/L	2.13 ± 0.84	2.72 ± 1.6	0.017 ± 0.014
	E	Law et al. (2011, 2012)	DO = 0.55 ± 0.05 mg-O_2/L Initial NH_4^+ = 500 mg-N/L pH=7	10.2 ± 0.106	5.43 ± 0.33	0.010 ± 0.0017
	F	Law et al. (2011, 2012)	DO = 0.55 ± 0.05 mg-O_2/L Initial NH_4^+ = 500 mg-N/L pH = 8	10.25 ± 0.049	6.7 ± 0.54	0.021 ± 0.0013
	G	Law et al. (2011, 2012)	DO = 1.25 ± 0.05 mg-O_2/L Initial NH_4^+ = 500 mg-N/L pH = 8	11.73 ± 0.042	11.28 ± 1.12	0.062 ± 0.01
Nitrite oxidation to nitrate by NOB 	H	Wunderlin et al. (2012, 2013)	DO = 1.1 ± 0.2 mg-O_2/L Initial NO_2^- = 15.5 mg-N/L	0.06 ± 0	0.09 ± 0.01 as nitrite uptake rate	0.007 ± 0.0002
Hydroxylamine oxidation to NOx 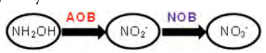	I	Wunderlin et al. (2012, 2013)	DO = 1.1 ± 0.2 mg-O_2/L Initial NH_2OH = 9.8 mg-N/L	0.04 ± 0.004	0.03 ± 0.013 as hydroxylamine uptake rate	0.002 ± 0.004

Table II. Fraction of nitrifying bacterial species in biomass (f^k) of the nine analysed experiments. Fractions values were calculated according to the community composition and species abundance information reported on each experiment publication listed on Table I. An error of 50% was assumed for each fraction value.

	Fraction of species (k) in experiment's biomass (Fraction ±50% error)								
	AOB				NOB				
Experiment ID	*Nitrosomonas europaea*	*Nitrosomonas eutropha*	*Nitrosospira multiformis*	*Nitrosococcus oceani*	*Nitrospira defluvii* (candidatus)	*Nitrobacter winogradskyi*	*Nitrobacter hamburgensis*	*Nitrospina gracilis*	Method for species detection and quantification
A	0.73 ± 0.36	0	0	0	0	0.135 ± 0.067	0.135 ± 0.067	0	qPCR
B	0.73 ± 0.36	0	0	0	0	0.135 ± 0.067	0.135 ± 0.067	0	qPCR
C	0.2 ± 0.1	0	0.3 ± 0.15	0	0.25 ± 0.125	0.125 ± 0.063	0.125 ± 0.063	0	Isotope signatures
D	0.6 ± 0.3	0.303 ± 0.15	0	0	0	0.045 ± 0.023	0.045 ± 0.023	0	qPCR
E	0.8 ± 0.4	0.05 ± 0.025	0.05 ± 0.025	0.05 ± 0.025	0.01 ± 0.005	0.01 ± 0.005	0.01 ± 0.005	0.01 ± 0.005	FISH
F	0.8 ± 0.4	0.05 ± 0.025	0.05 ± 0.025	0.05 ± 0.025	0.01 ± 0.005	0.01 ± 0.005	0.01 ± 0.005	0.01 ± 0.005	FISH
G	0.8 ± 0.4	0.05 ± 0.025	0.05 ± 0.025	0.05 ± 0.025	0.01 ± 0.005	0.01 ± 0.005	0.01 ± 0.005	0.01 ± 0.005	FISH
H	0.2 ± 0.1	0	0.3 ± 0.15	0	0.25 ± 0.125	0.125 ± 0.063	0.125 ± 0.063	0	Isotope signatures
I	0.2 ± 0.1	0	0.3 ± 0.15	0	0.25 ± 0.125	0.125 ± 0.063	0.125 ± 0.063	0	Isotope signatures

coefficient for metabolite i participating in reaction j. Mass balance in the network is maintained by imposing the condition $S \times v = 0$, where v is a vector of reaction rates v_j^k (or fluxes) (Feist et al., 2009; Varma and Palsson, 1994a). The reaction rate v_j^k is constrained as $\alpha_j^k \leq v_j^k \leq \beta_j^k$, where a_j and β_j represent imposed lower and upper limits (Varma and Palsson, 1994b) for a specific bacterial species k or the entire microbial community. FBA provides "snap-shot" estimates of the reaction rates v_j^k (Orth et al., 2010; Varma and Palsson, 1994a) by maximizing the rate of production of biomass for the microbial community, using $Z =$ maximize $v_{\mathrm{Ex-biomass}}^{\mathrm{COM}}$; where (Z) is the objective function of the optimization problem in FBA and $v_{\mathrm{Ex-biomass}}^{\mathrm{COM}}$ equals the sum of the biomass production rates of the eight modeled species.

Analyzing the Role of NO Redox Reactions on N_2O Formation

The effect of NO oxidation and reduction reactions on overall N_2O production by nitrifying communities was assessed by comparing the goodness of fit for simulations of different model variants to the nine experimental datasets. Those model variants that gave statistically similar estimates to measured values for cellular metabolism in the experimental studies, that is, the 38 variables listed in Table SI of *SI*, were deemed to be more accurate. The reactions of nitrogen respiration included in the nitrifying community network model are listed in Table III and Figure 3A shows the redox reactions that were included or excluded to create the eight model variants. Simulations of cellular metabolism in cultures were performed using these variants for each experimental dataset (Figure 3B). In order to capture uptake rates of substrates at species level, the observed sOUR and sAUR values (Table I) and the fraction of biomass as specific species (f^k, Table II) were used to obtain the rates of oxygen and ammonium uptake for each species k ($\beta_{\mathrm{O_2-Ex}}^k$ and $\beta_{\mathrm{NH_4-Ex}}^k$) as $\beta_{\mathrm{O_2-Ex}}^k = \mathrm{sOUR} \times f^k$ and $\beta_{\mathrm{NH_4-Ex}}^k = \mathrm{sAUR} \times f^k$. Then, the estimated $\beta_{\mathrm{O_2-Ex}}^k$ and $\beta_{\mathrm{NH_4-Ex}}^k$ values where used as input data (constraints) of the SMN model to perform FBA simulations. The set of f^k values for a particular experiment define the proportion of substrate (NH_4^+ and O_2) up taken by each species. A f^k value of zero resulted in null substrate uptake by the species k, consequently inactivating the species-specific SMN in the community model.

For each analyzed experiment using each model variant, a set of FBA simulations was performed following a Monte Carlo random sampling method in order to provide model estimates considering the uncertainty induced by the four input parameters sOUR, sAUR, f^k, and $\beta_{\mathrm{Cytaa3}}^{\mathrm{AOB}}$ (the rate of AOBs terminal oxidase cytochrome aa3). Each set of simulations consisted of 11,000 FBAs performed iteratively using as input data random combinations of values sampled from uniform probabilistic distributions of the four input parameters. Details of this procedure are specified on the section S3 of *SI*. The goodness of fit of the 8 model variants was assessed by fitting the model to data using the method described in our earlier publication (Perez-Garcia et al., 2014a), and illustrated in Figure 3B. The network fluxes obtained from each FBA were used in the formulas in Table SI of *SI* to estimate the values for the 38 variables characterizing the cellular metabolism at the moment of maximum N_2O productivity. To minimize the scale effect of different variables, the overall fit of model estimates to experimental data was quantified as absolute percent error (Δ) (Béchet et al., 2014; Makinia, 2010; Schuetz et al., 2007; van den Berg et al., 2006), calculated using the formula S1 in section S4 of *SI*.

Results and Discussion

Overview of Simulations Results

To predict the effect of diverse NO redox reactions on N_2O formation in nitrifying mixed cultures, we evaluate the performance of multispecies-model variants derived by systematically include or exclude equations of reactions catalyzed by Cyt_{P460}, Hmp, oxidative NirK, and Cyt554. Model variants providing accurate estimates of experimental datasets allowed to calculate the rates of the actual metabolic reactions occurring in the nitrifying cultures. Given that experimental datasets were obtained from the moment of cultures' maximum N2O productivity, estimations of time resolved

Table III. Bacterial species and reactions of nitrogen respiration included in the nitrifying community network model. Gray boxes indicate the presence of genes encoding for the reaction's catalytic enzyme in the genome of the corresponding species. Reactions for NO reduction to N_2O are indicated with symbol (+), NO oxidation reactions (not associated with hidorxilamine oxidoreductase (HAO)) are indicated with (*). Numbers in cells indicate the category of NO turnover reaction as specified in text and in Figure 1.

Stoichiometric equation of the model's nitrogen respiration reations		Enzyme name abreviation	Genes encoding for reaction's catalitic enzyme	Modeled species							
				AOB				NOB			
				Nitrosomonas europaea	*Nitrosomonas eutropha*	*Nitrosospira multiformis*	*Nitrosococcus oceani*	*C.* Nitrospira defluvii	*Nitrobacter winogradskyi*	*Nitrobacter hamburgensis*	*Nitrospina gracilis*
Species ID (as presented in KEGG database)				NMU	NET	NMU	NOC	NDE	NWI	NHA	NSP
$NH_3[p] + O_2[c] + Q8H_2[c] \rightarrow NH_2OH[p] + Q8[c] + H_2O[c]$		AMO	*amoABC*								
$NH_3[p] + N_2O_4[p] + Q8H_2[c] \rightarrow NH_2OH[p] + H_2O[c] + Q8[c] + 2\ NO[p]$		AMO	*amoABC*								
$NH_2OH[p] + Cyt554[p] \rightarrow NOH[p] + Cyt554e[p] + 2\ H^+[p]$		HAO	*haoAB*								
$NOH[p] + 0.5\ Cyt554[p] \rightarrow NO[p] + 0.5\ Cyt554e[p] + H^+[p]$		HAO	*haoAB*								
$NO[p] + 0.5\ Cyt554[p] + H_2O[p] \rightarrow HNO_2[p] + 0.5\ Cyt554e[p] + H^+[p]$		HAO	*haoAB*								
$0.5\ O_2[c] + 4\ H^+[c] + 2\ Cyt552e[p] \rightarrow H_2O[ac] + 2\ H^+[p] + 2\ Cyt552[p]$		Cyt_{aa3}	*coxABC*								
$HNO_2[p] + 3\ H^+[c] + 3\ Cyt552e[p] \rightarrow 0.5\ N_2[p] + 2\ H_2O[p] + 3\ Cyt552[p]$		Cyt_{aa3}	*coxA2*								
$HNO_2[p] + Cyt552e[p] + H^+[p] \rightarrow NO[p] + Cyt552[p] + H_2O[p]$		NirK	*nirK*								
$NO[p] + 0.5\ NAD[c] + H_2O[c] \rightarrow NO_2^-[p] + 0.5\ NADH[c] + 1.5\ H^+[p]$	*	NirK	*nirK*						(2)		
$0.5\ NH_2OH[p] + 0.5\ NO[p] + 2\ Cyt552[p] + H_2O[p] \rightarrow HNO_2[p] + 2\ Cyt552e[p] + 4\ H^+[p]$	*	Cyt_{P460}	*cyp*	(1)	(1)						
$NO[p] + Cyt552[p] + H_2O[p] \rightarrow HNO_2[p] + Cyt552e[p] + H^+[p]$	*	Cyt_{P460}	*cyp*							(2)	(2)
$NO[c] + O_2[c] + 0.5\ NADH[c] \rightarrow NO_3[c] + 0.5\ NAD[c] + 0.5\ H^+[c]$	*	Hmp	*hmp*		(1)		(1)	(2)			
$NO[c] + H^+[c] + 0.5\ NADH[c] \rightarrow 0.5\ N_2O[c] + 0.5\ H_2O[c]$	+	Hmp	*hmp*								
$NO[p] + Cyt552e[p] + H^+[p] \rightarrow 0.5\ N_2O[p] + Cyt552[p] + 0.5\ H_2O[p]$	+	cNor	*norABC*							(3)	
$NO[p] + H^+[p] + 0.5\ Cyt554e[p] \rightarrow 0.5\ N_2O[p] + 0.5\ Cyt554e[p] + 0.5\ H_2O[p]$	+	Cyt_{554}	*cycA*					(3)			
$NO_2^-[c] + 2\ Cyt550[c] + H_2O[c] \leftrightarrow NO_3^-[c] + 2\ Cyt550e[c] + 2\ H^+[c]$		cNXR	*nxrA-K*								
$NO_2^-[p] + 2\ Cyt550[c] + H_2O[p] \rightarrow NO_3^-[p] + 2\ Cyt550e[c] + 2\ H^+[p]$		pNXR	*nxrACB*								
$0.5\ O_2[c] + 4\ H^+[c] + 2\ Cyt550e[c] \rightarrow H_2O[c] + 2\ H^+[p] + 2\ Cyt550[c]$		Cyt_{aa3}	*cydABC*								
$0.5\ O_2[c] + 2\ H^+[c] + 2\ Cyt550e[c] \rightarrow H_2O[c] + 2\ Cyt550[c]$		Cyt_{aa3}	*cydABC*								
$NO_2^-[p] + Cyt550e[c] + 2\ H^+[p] \rightarrow NO[p] + Cyt550[c] + H_2O[p]$		NirK	*nirK*								
$NO_3^-[p] + NADH[c] + H^+[c] \rightarrow NO_2^-[p] + NAD[c] + H_2O[c]$		pNXR	*nxrAB*								
$NO_2^-[p] + Q8H_2[c] \rightarrow NO_3^-[p] + Q8[c] + H_2O[c]$		NAR	*narGHJI*								
$NO_2^-[c] + 4\ H^+[c] + 3\ NADH[c] \rightarrow NH_3[c] + 2\ H_2O[c] + 3\ NAD[c]$		NirB	*nirB*								
$NO_2^-[c] + 6\ Fee[c] + 7\ H^+[c] \leftrightarrow NH_3[c] + 2\ H_2O + 6\ Fe[c]$		NirA	*nirA*								
Genome publication reference				(Chain et al., 2003)	(Stein et al., 2007)	(Norton et al., 2008)	(Klotz et al., 2006)	(Lücker et al., 2010)	(Starkenburg et al., 2006)	(Starkenburg et al., 2008b)	(Lücker et al., 2013)

[p] = metabolic compound in periplasmic space subcompartment. [c] = metabolic compound in cytoplasmic space subcompartment.

concentrations of nitrogenous compounds were not necessarily. As shown in Figure 4, Simulations show that including NO oxidation reactions in AOB and NOB metabolic networks significantly improves model fitness to experimental data. The simulation of ammonia oxidation to nitrate by AOB and NOB shows that NO oxidation in AOB occurs in nitrifying cultures when the dissolved oxygen (DO) exceeds 1.9 ± 0.2 mg/L (experiments A and C), while for cultures transitioning from full to partial nitrification (experiment B with DO lowered from 3.8 to 1.5 mg-O_2/L), NO oxidation occurs in both AOB and NOB. This is caused by a lack of electron acceptor O_2, which leads to NO production by AOB and subsequent NO oxidation by NOB. Simulations of ammonia oxidation to nitrite by AOB (experiments D, E, F, and G) also show that during partial nitrification (DO of 1.25–0.5 mg-O_2/L) NO is oxidized to NO_2^- by AOB. On the other hand, simulations of processes of nitrite oxidation to nitrate by NOB (experiment H) and hydroxylamine oxidation to NOx (experiment I) show that NO oxidation does not occur under these conditions. Simulations also indicate that NOB do not produce N_2O during ammonia oxidation to nitrate or nitrite.

Model Variants Fitness

Figure 4 shows a heatmap of absolute percent errors (Δ) scores, ranging from 19.9% to 179.9%, obtained with the eight model variants fitting the nine experimental datasets. A lower Δ value represents more accurate simulations; $\Delta = 0$ % means a perfect fit of the experimental dataset by the model while $\Delta \geq 100\%$ means that estimates that has an error that doubles the experimental values. SMN models for single species used to fit one to ten metabolic variables typically show absolute errors ranging from 5% to 45% (Schuetz et al., 2007; Stolyar et al., 2007). The reported errors for the SMN model arise from the inclusion or exclusions of NO redox reactions, from biological phenomena that were not modeled (such as enzyme substrate affinity and metabolite accumulation), and the use of biomass maximization as the objective function. A Δ value of $<45\%$ indicates that the SMN model was able to simultaneously fit observations for 17–31 variables in nine experimental studies with a maximum deviation of 45%. We therefore consider simulations with $\Delta < 4$ % to provide a good representation of the metabolic activities occurring in the experimental cultures.

The model variants influenced fitness scores of both, complete datasets (Δ scores, evaluating 17–31 variables) and individual variables. To illustrate this, Figure 5 presents the absolute error (defined as $\left|X_t^{\exp} - X_t^{\text{est}}\right| / X_t^{\exp}$) of all variables estimated for experiments A, B, and G—which are representative cases of analyzed nitrification processes—using model variants 8, 6, and 5. Variants 6 and 5 provide the lowest Δ scores for processes of ammonium oxidation to nitrate and nitrite, while variant 8 is considered the base case scenario in which no NO redox reactions were included. Figure 5 illustrates that in the simulations for experiment A the inclusion of NO oxidation reactions in AOB (variant 6) decreased the error in estimates for N_2O-N and NO-N production rates (indicated with arrows in Figure 5). Similarly, variant 6 decreased the error in estimated N_2O-N production rates

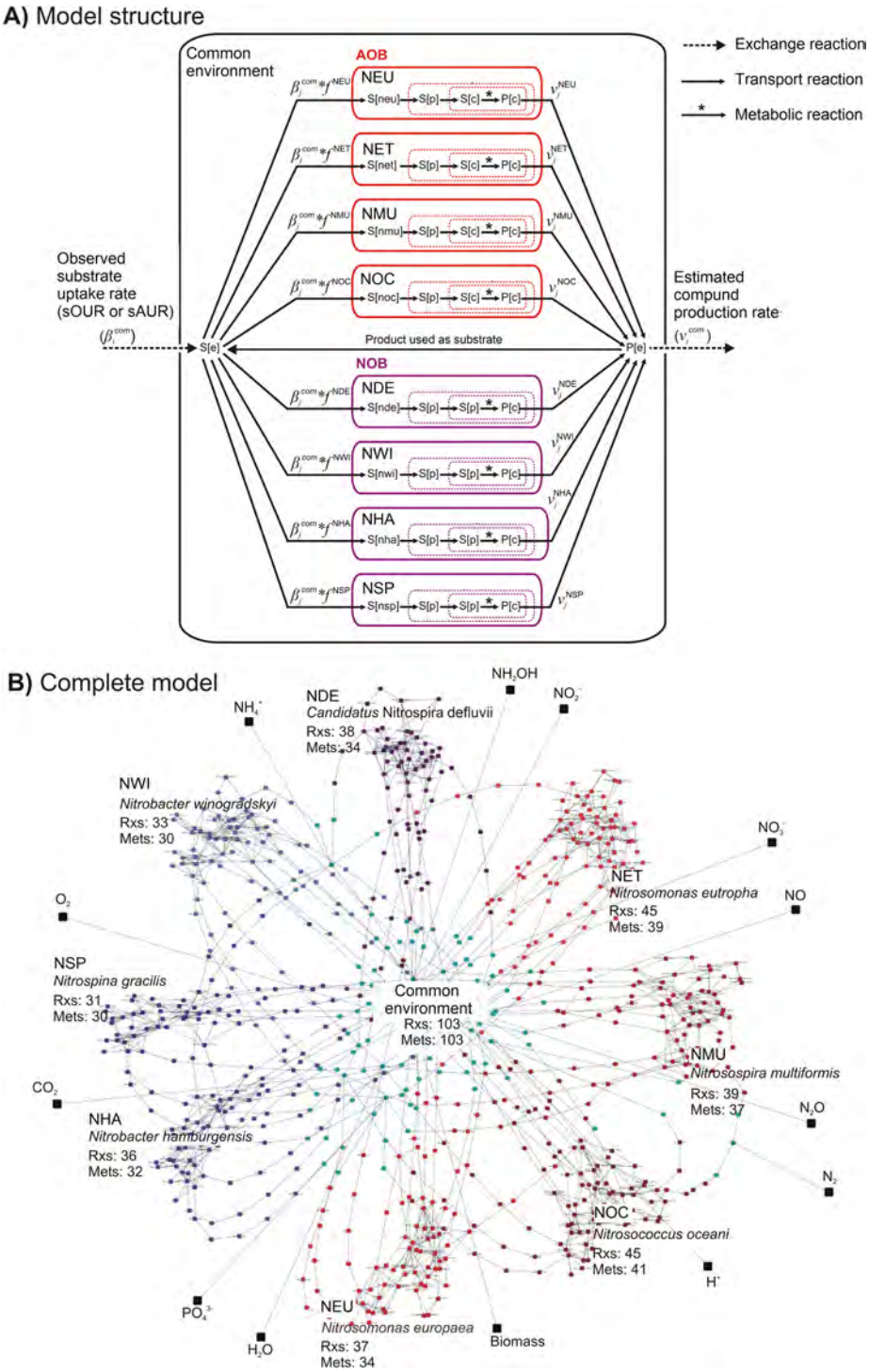

Figure 2. Nitrifying community metabolic network model. **A**: Diagram of the multi-compartmentalized structure of the network model. Each species is modeled as a compartment (horizontal boxes) of the same model which contains a species-specific metabolic network distributed in three sub-compartments (delimited by dashed line boxes) that represent cell's extracellular [species ID] periplasmic [p] and cytoplasmic [c] spaces. Each species-specific compartment exchange substrate (S) and product (P) compounds with a "Common environment" compartment [e] (out most external box). Community substrate uptake rates (i.e., sOUR and sAUR) are corrected with f^k values (fraction of species k per gram of community biomass). **B**: Complete nitrifying community metabolic network formed with 787 nodes representing 407 reactions and 380 metabolic compounds. Species-specific nodes form clusters (eight) around community nodes. Big nodes at the periphery of the network represent the exchange reactions for uptake and secretion of compounds outside of the community.

A) Tested model variants

Variant number	NO reduction to N_2O by NOB	NO oxidation to NO_2^- by AOB	NO oxidation to NO_2^- by NOB
1	Included	Included	Included
2	Included	Included	Excluded
3	Included	Excluded	Included
4	Included	Excluded	Excluded
5	Excluded	Included	Included
6	Excluded	Included	Excluded
7	Excluded	Excluded	Included
8	Excluded	Excluded	Excluded

B) Scheme of simulation study workflow

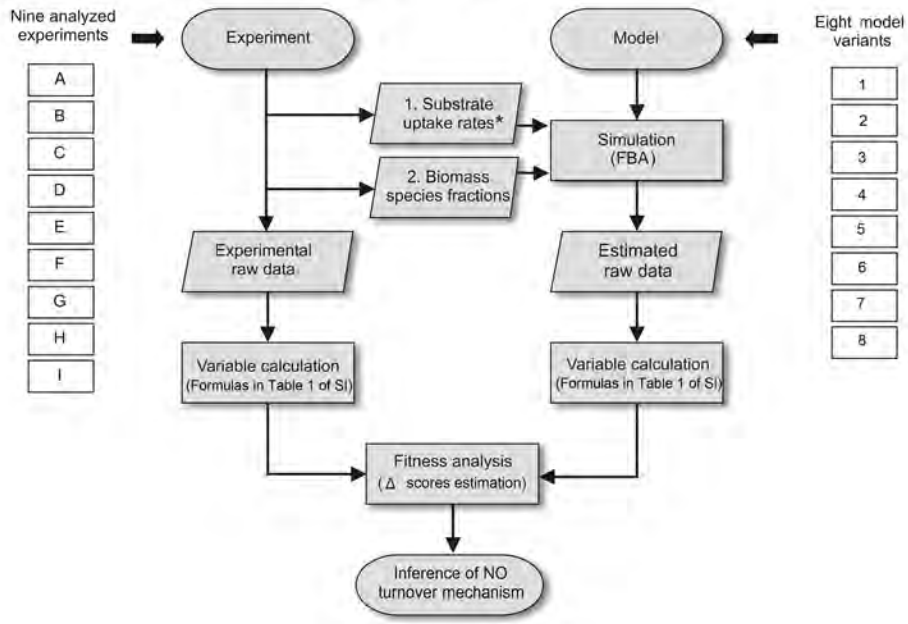

Figure 3. Research approach: (**A**) Tested model variants, variants were derived by systematically include or exclude equations for NO redox reactions in model formulation. (**B**) Research workflow for SMN model driven analysis of nitrification experiments.

in simulations of ammonium oxidation to nitrite by AOB (experiment G). Variant 5 (which includes NO oxidation in AOB and NOB) decreased the error in the estimated N_2O-N/NH_4^+-N yield for community and the NO-N and N_2O-N production rates for experiment B. Additionally, the results in Figure 5 indicate that the multispecies SMN model accurately estimated values of variables such as *N. europaea* fraction in biomass, the efficiency of NH_4^+-N oxidation to NO_3^--N by community, and the sOUR of the whole community and the AOB fraction.

NO Oxidation to NO_2^- by AOB

Simulations of both ammonia oxidation to nitrate (experiments A, B, and C) and ammonia oxidation to nitrite (experiments D, E, F, and G) show that only model variants which include NO oxidation are capable of fitting observations with sufficient accuracy. Model variants including reactions for NO oxidation in AOB but not NOB (variants 2 and 6) achieve the lowest error in fitting data for ammonia oxidation to nitrate at DO $> 1.9 \pm 0.2$ mg-O_2/L. Both of the variants 2 and 6 show identical performance (Figure 4) with Δ scores of $19.6 \pm 3.4\%$ and $42.2 \pm 2.8\%$ for experiments A and C, respectively, indicating that including N_2O production by NOB does not affect model fitness. Similarly, ammonia oxidation to nitrite (experiments D, E, F, and G) is better simulated by including NO oxidation by AOB but not NOB. Figure 4 shows that variants 2 and 6 show similar performance achieving high fitness Δ scores for experiments D $= 33.6 \pm 2.8$, E $= 33.6 \pm 9.6$, F $= 28.6 \pm 10.2$, and G $= 25.8 \pm 8.0\%$. The inclusion of NO oxidation by AOB does not

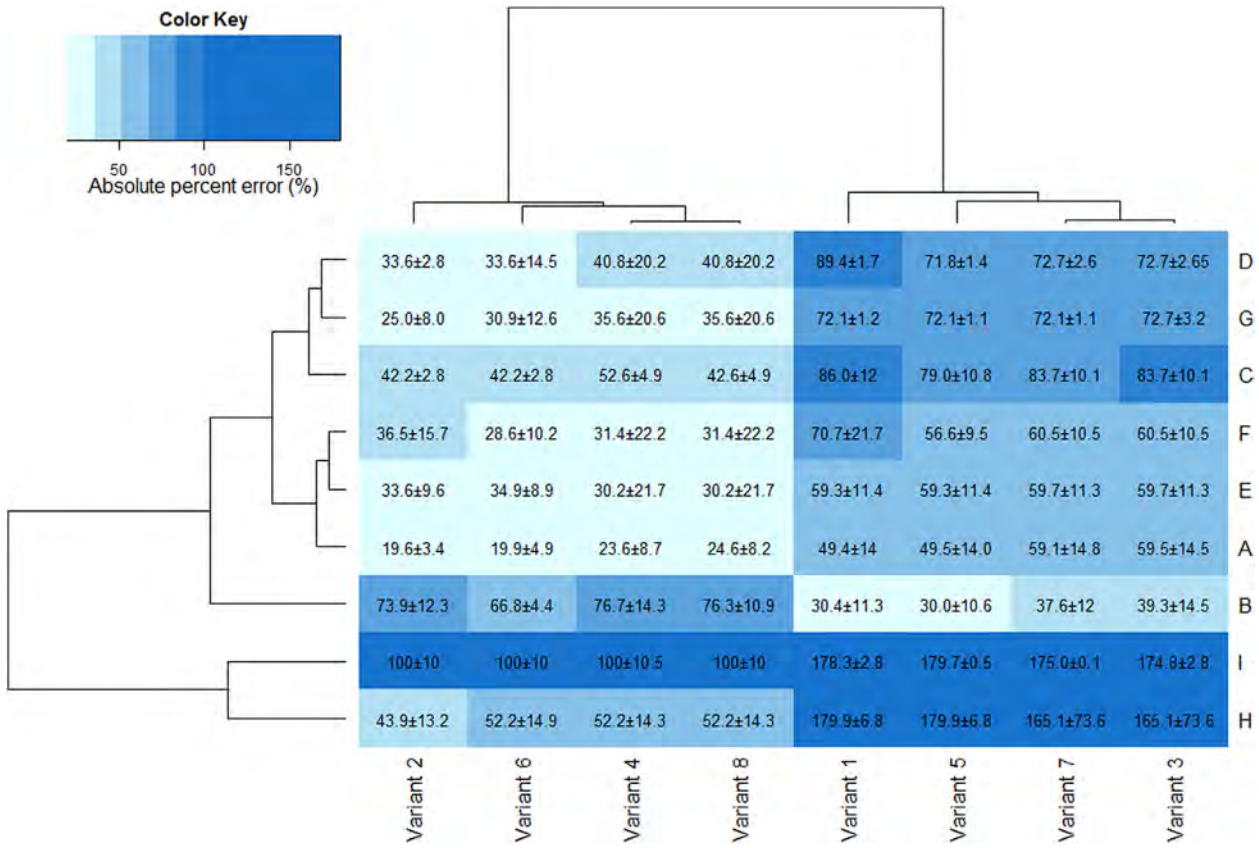

Figure 4. Absolute percent error (Δ) of eight models variants used to estimate nine experimental datasets (letters A to I). More accurate variants (less error) have lower scores. Each cell contains the mean and standard deviation resulting from the 12,000 FBAs ran using the sampled values from the uniform probability distribution of model's input parameters.

improve the model's fit to data in experiments involving NO_2^- oxidation to NO_3^- (H) and NH_2OH oxidation to NO_X (experiment I), suggesting that under such circumstances NO oxidation might be insignificant.

NO Oxidation to NO_2^- by NOB

Figures 4 and 5 show that model variants which included the reactions for NO oxidation in NOB (variants 1, 3, 5, and 7) achieved low fitness (high Δ scores) to data from all experiments except experiment B; this dataset was better simulated with variants that included reactions of NO oxidation in both AOB and NOB (i.e., variants 1 and 5). Both variants showed similar fits to experiment B (Figure 4, $\Delta = 30.4 \pm 11.3$ and 30.4 ± 10.3 for variant 1 and 5, respectively) indicating that N_2O production by NOB is insignificant. Experiment B dataset was obtained from a culture transitioning from full to partial nitrification and showed high N_2O and NO production (respectively 0.071 ± 0.025 and 0.003 ± 0.0005 mmol-N/g-COD*h). In this experiment the culture underwent a transition from full to partial nitrification, which was achieved by decreasing the dissolved oxygen and sludge retention time (Ahn et al., 2011). Our simulations indicate that NOB are metabolically active under these conditions and responsible for oxidizing the NO produced by AOB.

NO Reduction to N_2O by NOB

None of the model variants that included the reactions for NO reduction to N_2O by NOB (variants 5, 6, 7, and 8) showed improved fitness scores over variants that excluded these reactions. For example, simulations of experiments involving ammonium oxidation to nitrate (A, B, and C) resulted in zero rate of N_2O production by NOB irrespective of whether those reactions were included or excluded during model formulation. This indicates that from the perspective of mass and energy balance it is unlikely that NOB produced the observed N_2O in the above experiments. By contrast, experiment H involving NOB oxidation of NO_2^- to NO_3^- shows N_2O production (Wunderlin et al., 2012, 2013). Model simulations support these experimental observations ($\Delta = 43.9 \pm 13.2\%$); only variant 2, which included reactions for NO reduction by cNor and Cyt_{554} in NOB (i.e., N_2O production by NOB), reproduces the experimentally observed sN_2OPR values, suggesting cNor activity in NOB.

Effect of Alternative NO Redox Reactions on N_2O Formation

Figure 6 compares the experimental N_2O production rates (sN_2OPR) to estimates from variants 5, 6, and 8 (sN_2OPR estimates

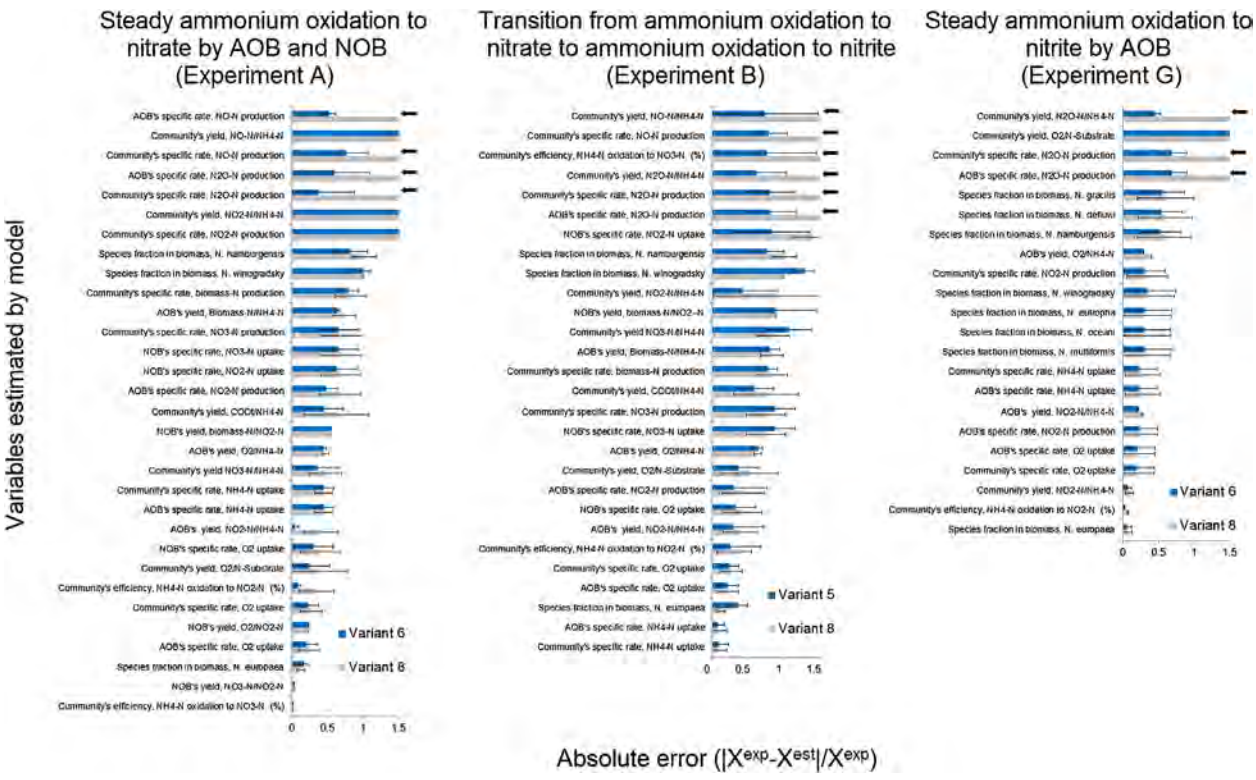

Figure 5. Absolute error of variables estimated by model variants used to estimate datasets from experiments A, B, and G. The figure shows three independent fitness analysis, each of them performed for each experimental dataset. Model variant 8 captures the base case scenario where reactions of NO oxidation to NO_2^- associated to both AOB and NOB do not occur in nitrification systems. Variables not showing data were not estimated for that particular experimental dataset. Steady ammonium oxidation to nitrite by AOB (Experiment G).

for experiments H and I were zero and are not shown). Model variant 8—base case scenario that excludes the alternative NO redox reactions being tested—significantly over estimates sN_2POR values for all experiments. In contrast, the sN_2OPR estimates of variant 6, which including NO oxidation to NO_2^- by AOB, show statistical similarity to experimental values for experiments involving ammonium oxidation to nitrate and nitrite. For example, sN_2OPR estimates for ammonium oxidation to nitrate (experiments A and B) range from 0.004 to 0.11 mmol-N $gCOD^{-1}$ h^{-1} without having statistical significant differences to experimental observations (according to *t*-test at $\alpha = 0.05$). Furthermore, simulations that include NO oxidation by NOB (variant 5) underestimate sN_2OPR values, except in experiments on transitioning between full and partial nitrification (experiment B). All sN_2OPR estimates for variants that excluded NO oxidation reactions (variants 3, 4, 7, and 8) were significantly higher than experimental rates (data not shown). The simulations indicate that NO oxidation by Cyt_{P460} and Hmp can lower N_2O formation during ammonia oxidation to nitrite and nitrate by as much as 60–86.4%; however this reduction is not seen during NH_2OH and nitrite oxidation (experiment I). None of variants tested showed satisfactory fitness to datasets for NH_2OH oxidation to NOx by AOB and NOB (experiment I) indicating that the proportion between NO_2^-, NO and N_2O products differs significantly form that that observed during NH_4^+ oxidation. Possibly due an excess of electron equivalents in AOB cells due the bypassing of the reaction catalyzed by AMO enzyme, which is a major electron equivalent sink.

The rate of O_2 consumption by the terminal oxidase cytochrome aa3 (β^{AOB}_{Cytaa3}) in AOB is a key parameter for fitting the experimental sN_2OPR values as this reaction determines the amount of electron equivalents available to reduce NO_2^- and NO to N_2O by NirK and cNor (Perez-Garcia et al., 2014b). Other mathematical modeling studies similarly highlight the role of terminal oxidase rate in AOB on the N_2O formed during nitrification (Ni et al., 2013). Figure S1 of *SI* shows the influence of model variants on the relationship between β^{AOB}_{Cytaa3} and sN_2OPR; variants that include NO oxidation reactions (variants 6 and 8) make the model less sensitive to changes of sOUR values. Results from Figure S1 indicate that the reaction rates of the terminal oxidase must be the 20–50 % of the observed sOUR in order to activate N_2O production as electron sink mechanism. Figure S1 also shows that low variations in β^{AOB}_{Cytaa3} reatly affect sN_2OPR value during ammonium oxidation to nitrite (e.g., in experiment F). This happens because the accumulation of NO_2^- and NO enables them to be rapidly used as acceptors of electrons not used by the terminal oxidase (Cytaa3).

In agreement with the observations of Ahn et al. (2011) and Yu et al. (2010) our simulations estimate larger NO and N_2O production during ammonium oxidation to nitrite compared to ammonium oxidation to nitrate (Figure 6, middle graph). The exception was experiment B in which the culture transitioned from

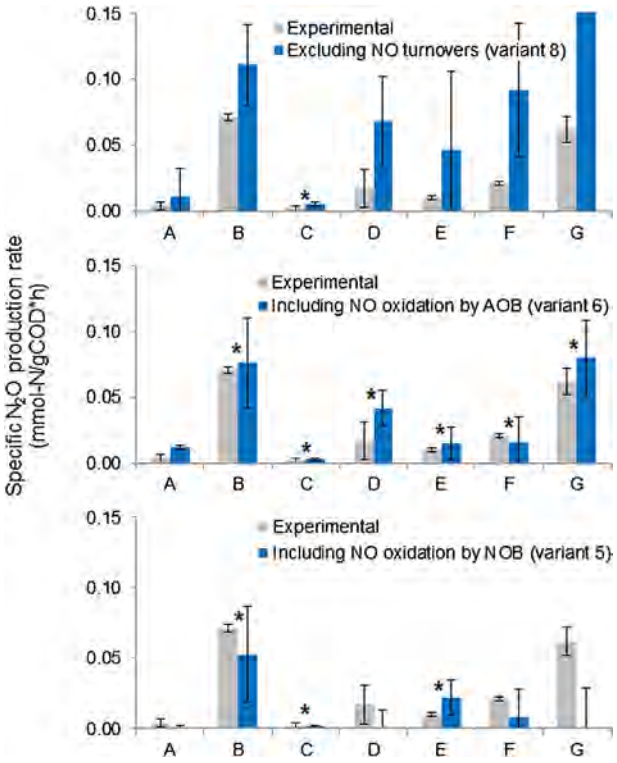

Figure 6. Experimental and estimated specific N_2O-N production rates (sN_2OPR). Each graph presents the sN_2OPR observed on experiments (gray bars) and the estimations obtained from one of the model variants 8 (top), 6 (middle), or 5 (bellow). Stars on top of bars indicate no significant difference between experimental and observed sN_2OPR according to *t*-test at $\alpha = 0.05$.

complete to partial nitrification as in this experiment NirK mediated N_2O production by AOB would dominate (Perez-Garcia et al., 2014b; Yu et al., 2010). The above results indicate two modes of N_2O production: i) when the culture is at steady state N_2O is expected to be produced constantly at minor quantities, majorly through the HAO mediated pathway; in contrast ii) when the cultures changes to a different concentrations of electron donor or acceptor N_2O is produced ephemerally (few minutes) but in large quantities, majorly through NirK mediated pathway. Ammonium oxidation to nitrate showed lower N_2O production than ammonium oxidation to nitrite because NOB avoid nitrite accumulation, which it is used by AOB as terminal electron acceptor in reactions catalyzed by nitrite and nitric oxide reductase (NirK and cNor), accompanied with N_2O production (Ahn et al., 2010; Kampschreur et al., 2009; Schreiber et al., 2012). Additionally, our fitness analysis suggests that NOB can oxidize NO produced by AOB. Consequently, NOB decrees N_2O production by reducing the substrate (NO) available for cNor enzyme in AOB. According to these results, N_2O emission mitigation strategies would involve the maintenance of a rich NOB population in nitrifying bioreactors. NO easily diffuses through cell membranes due its hydrophobicity and small size (Rocha et al., 2010) and AOB and NOB populations have been reported to grow in close proximity in activated sludge flocs (Daims et al., 2006; Kindaichi et al., 2004). As a result, in a complete mixed nitrifying culture diffusion of NO from AOB to NOB would be rapid, therefore enabling mutualistic NO oxidation by NOB. In addition, as NO is cytotoxic (Richardson et al., 2009) and may inhibit nitrite oxidation by NOB (Courtens et al., 2015), therefore it is possible that survival may require detoxification by these organisms via production enzymes to actively reduce or oxidize NO. Therefore, the occurrence of NO oxidation reactions in AOB and NOB would provide an advantage by extracting electron equivalents while reducing toxic damage by this molecule. Nevertheless, NO oxidation by NOB cells requires to be confirmed on laboratory and full scale wastewater treatment systems.

Effect of Community Composition on N_2O Production

Changes in sN_2OPR estimates for different combinations of NO and N_2O production/consumption pathways show that speciation of AOB and NOB populations affect N_2O production. Therefore, the selection of sludge sources to start nitrifying cultures and the operational ammonium and nitrite concentrations that maintain specific AOB and NOB populations would be important factors to consider on the design of operational strategies to mitigate N_2O emissions. Simulations results presented in Figure 7 suggest that in experiments D, E, F, and G over 60% of N_2O was produced by *N. eutropha* and 40% by *N. europaea*, although it constituted a smaller fraction of biomass (f^{NET} between 0.3 ± 0.15 and 0.05 ± 0.025) than *N. europaea* (f^{NEU} between 0.6 ± 0.3 and 0.8 ± 0.4). This is attributed to *N. eutropha* having multiple enzymes (i.e., Hmp, Cyt_{554} and cNor) for catalyzing the reduction of NO to N_2O. Accordingly, nitrifying microbial communities dominated by *N. eutropha* produce more N_2O than the ones dominated by *N. europaea*. Furthermore, NOB communities dominated by *Nitrobacter* spp. would be better at mitigating N_2O emission during ammonium oxidation to nitrate; the presence of genes encoding for NirK and Cyt_{P460} in their genomes suggests that this genus can catalyse more diverse reactions for oxidizing NO to NO_2^-. Indeed, Courtens et al. (2015) showed that NO_2^- oxidization in sludge dominated by *Nitrobacter* spp. shows lower inhibition by NO in comparison to *Nitrospira* spp. dominated sludge. This N_2O emission mitigation mechanism could be particularly important in wastewater streams containing high nitrogen load as *Nitrobacter*-like bacteria dominate the NOB populations in these environments (Daims and Wagner, 2010). Nevertheless, the occurrence of this N_2O mitigation mechanism requires experimental verification through NirK, CytP460, Cyt554, and Hmp gene expression measurements or flux measurements using isotopic labeling of nitrogenous species.

The computational approach developed in this research allows modeling microbial communities with different species richness and abundances, and quantifying the exchange of metabolic compounds between such species. Such approach can be particularly relevant to evaluate inoculation/bioaugmentation strategies and the productivity of nitrogenous species under different feeding regimes. The SMN model present herein can be directly expanded with kinetic and differential equations related to be able to predict nitrogen conversion profiles during the whole experimental course, similarly as those predicted by the Activated Sludge Models (ASM) (van Loosdrecht et al., 2008). Also, inclusion of coefficients for gas-liquid mass transfer as well as processes for

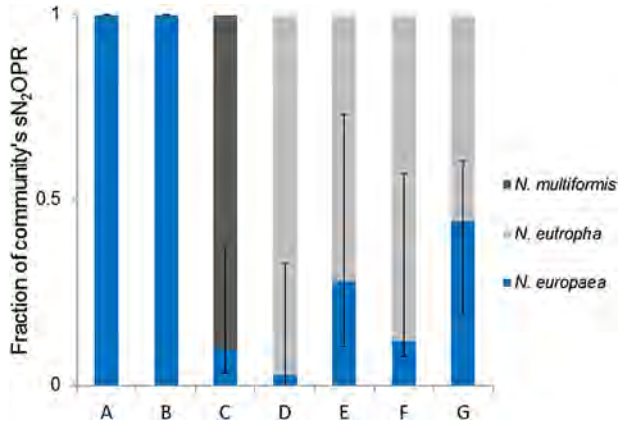

Figure 7. Fraction of N_2O produced in each analyzed experiment by *N. europaea*, *N. eutropha*, and *N. multiformis*. Break on bars indicate the mean fractions, while whiskers indicate the estimated fraction range.

cell decay and lysis will improve model capacity to assist on the design of bioreactor operation strategies to mitigate N_2O emissions. Finally the model presented herein can be further applied to interpret observed profiles of relevant genes, proteins (Lewis et al., 2010) and metabolites (Kümmel et al., 2006), therefore providing a computational platform to engineer nitrifying processes on basis of deep biological.

Conclusions

This study demonstrates that the metabolism of different populations of AOB and NOB species in nitrifying mixed cultures can be modeled and simulated using genome-informed metabolic network models and flux balance analysis together with species-level community population profiles and process performance measurements. The modeling approach presented in this study can be used to develop or test microbial ecology and metabolic hypothesis of nitrifying communities. The results highlight that NO oxidation to NO_2^- by Cyt_{P460}, Hmp and NirK in AOB could potentially be active during nitrification, and be a mechanism for decreasing the amount of N_2O formed in these systems. Results also show that the NO produced by AOB during the transition from full to partial nitrification could be taken up by NOB and oxidized to NO_2^- by NirK. By consuming NO_2^- and NO produced by AOB, NOB have the ability to lower the amount of N_2O formed; in this case both molecules are used as electron donors in NOB metabolism. None of our simulation supports the activation of NO reduction to N_2O in NOB. In summary the composition of AOB and NOB species in the microbial population and its particular pool of isozymes affect the amount of N_2O produced during nitrification.

The valuable intellectual feedback from Professors Bart Smets and Benoit Guieysse substantially improved the quality of this study. OP-G was supported by scholarships from The University of Auckland and The Mexican National Council for Science and Technology (CONACyT). OP-G thanks Dr Diana Spratt Casas for editorial improvement.

References

Ahn JH, Kim S, Park H, Rahm B, Pagilla K, Chandran K. 2010. N_2O emissions from activated sludge processes, 2008–2009: Results of a national monitoring survey in the united states. Enviro Sci Technol 44:4505–4511.

Ahn JH, Kwan T, Chandran K. 2011. Comparison of partial and full nitrification processes applied for treating high-strength nitrogen wastewaters: Microbial ecology through nitrous oxide production. Enviro Sci Technol 45:2734–2740.

Béchet Q, Shilton A, Guieysse B. 2014. Full-scale validation of a model of algal productivity. Enviro Sci Technol 48:13826–13833.

Chaganti SR, Kim D-, Lalman JA. 2011. Flux balance analysis of mixed anaerobic microbial communities: Effects of linoleic acid (LA) and pH on biohydrogen production. Int J Hydrogen Energy 36:14141–14152.

Chain P, Lamerdin J, Larimer F, Regala W, Lao V, Land M, Hauser L, Hooper A, Klotz M, Norton J, Sayavedra-Soto L, Arciero D, Hommes N, Whittaker M, Arp D. 2003. Complete genome sequence of the ammonia-oxidizing bacterium and obligate chemolithoautotroph Nitrosomonas europaea. J Bacteriol 185:2759–2773.

Courtens ENP, De Clippeleir H, Vlaeminck SE, Jordaens R, Park H, Chandran K, Boon N. 2015. Nitric oxide preferentially inhibits nitrite oxidizing communities with high affinity for nitrite. J Biotechnol 193:120–122.

Daims H, Wagner M. 2010. The microbiology of nitrogen removal. In: Seviour RJ, Nielsen PH, editors. Microbial ecology of activated sludge. London: IWA Publishing. p 259–280.

Daims H, Taylor MW, Wagner M. 2006. Wastewater treatment: A model system for microbial ecology. Trends Biotechnol 24:483–489.

Dias JML, Serafim LS, Lemos PC, Reis MAM, Oliveira R. 2005. Mathematical modelling of a mixed culture cultivation process for the production of polyhydroxybutyrate. Biotechnol Bioeng 92:209–222.

Elmore BO, Bergmann DJ, Klotz MG, Hooper AB. 2007. Cytochromes P460 and c'-beta; A new family of high-spin cytochromes c. FEBS Lett 581:911–916.

Feist AM, Herrgård MJ, Thiele I, Reed JL, Palsson BØ. 2009. Reconstruction of biochemical networks in microorganisms. Nat Rev Microbiol 7:129–143.

Foley J, de Haas D, Yuan Z, Lant P. 2010. Nitrous oxide generation in full-scale biological nutrient removal wastewater treatment plants. Water Res 44:831–844.

Grady CPLJ, Daugger GT, Lim HC. 1999. Biological wastewater treatment. New York: Marcel Dekker.

Kampschreur MJ, Picioreanu C, Tan N, Kleerebezem R, Jetten MSM, Van Loosdrecht MCM. 2007. Unraveling the source of nitric oxide emission during nitrification. Water Environ Res 79:2499–2509.

Kampschreur MJ, Tan NCG, Kleerebezem R, Picioreanu C, Jetten MSM, Van Loosdrecht MCM. 2008. Effect of dynamic process conditions on nitrogen oxides emission from a nitrifying culture. Enviro Sci Technol 42:429–435.

Kampschreur MJ, Temmink H, Kleerebezem R, Jetten MSM, van Loosdrecht MCM. 2009. Nitrous oxide emission during wastewater treatment. Water Res 43:4093–4103.

Kindaichi T, Ito T, Okabe S. 2004. Ecophysiological interaction between nitrifying bacteria and heterotrophic bacteria in autotrophic nitrifying biofilms as determined by microautoradiography-fluorescence in situ hybridization. Appl Environ Microbiol 70:1641–1650.

Klitgord N, Segrè D. 2010. Environments that induce synthetic microbial ecosystems. PLoS Comput Biol 6:e1001002.

Klotz MG, Arp DJ, Chain PSG, El-Sheikh AF, Hauser LJ, Hommes NG, Larimer FW, Malfatti SA, Norton JM, Poret-Peterson AT, Vergez LM, Ward BB. 2006. Complete genome sequence of the marine, chemolithoautotrophic, ammonia-oxidizing bacterium Nitrosococcus oceani ATCC 19707. Appl Environ Microbiol 72:6299–6315.

Kümmel A, Panke S, Heinemann M. 2006. Putative regulatory sites unraveled by network-embedded thermodynamic analysis of metabolome data. Mol Sys Biol 2:0034.

Law Y, Lant P, Yuan Z. 2011. The effect of pH on N_2O production under aerobic conditions in a partial nitritation system. Water Res 45:5934–5944.

Law Y, Ni B, Lant P, Yuan Z. 2012. N2O production rate of an enriched ammonia-oxidising bacteria culture exponentially correlates to its ammonia oxidation rate. Water Res 46:3409–3419.

Lewis NE, Hixson KK, Conrad TM, Lerman JA, Charusanti P, Polpitiya AD, Adkins JN, Schramm G, Purvine SO, Lopez-Ferrer D, Weitz KK, Eils R, König R, Smith

RD, Palsson BØ. 2010. Omic data from evolved *E. coli* are consistent with computed optimal growth from genome-scale models. Mol Sys Biol 6:390.
Lücker S, Nowka B, Rattei T, Spieck E, Daims H. 2013. The genome of Nitrospina gracilis illuminates the metabolism and evolution of the major marine nitrite oxidizer. Frontiers in Microbiology 4:27.
Lücker S, Wagner M, Maixner F, Pelletier E, Koch H, Vacherie B, Rattei T, Damsté JSS, Spieck E, Le Paslier D, Daims H. 2010. A Nitrospira metagenome illuminates the physiology and evolution of globally important nitrite-oxidizing bacteria. Proc Natl Acad Sci USA 107:13479–13484.
Makinia J. 2010. Mathematical modelling and computer simulation of activated sludge systems. London, UK: IWA Publishing.
Mampaey KE, Beuckels B, Kampschreur MJ, Kleerebezem R, Van Loosdrecht MCM, Volcke EIP. 2013. Modeling nitrous and nitric oxide emissions by autotrophic ammonia-oxidizing bacteria. Environ Technol 34:1555–1566.
Ni B-, Ye L, Law Y, Byers C, Yuan Z. 2013. Mathematical modeling of nitrous oxide (N_2O) emissions from full-scale wastewater treatment plants. Enviro Sci Technol 47:7795–7803.
Norton JM, Klotz MG, Stein LY, Arp DJ, Bottomley PJ, Chain PSG, Hauser LJ, Land ML, Larimer FW, Shin MW, Starkenburg SR. 2008. Complete genome sequence of Nitrosospira multiformis, an ammonia-oxidizing bacterium from the soil environment. Appl Environ Microbiol 74:3559–3572.
Numata M, Saito T, Yamazaki T, Fukumori Y, Yamanaka T. 1990. Cytochrome P-460 of Nitrosomonas europaea: Further purification and further characterization. J Biochem 108:1016–1021.
Orth JD, Thiele I, Palsson BO. 2010. What is flux balance analysis? Nat Biotechnol 28:245–248.
Pardelha F, Albuquerque MGE, Reis MAM, Dias JML, Oliveira R. 2012. Flux balance analysis of mixed microbial cultures: Application to the production of polyhydroxyalkanoates from complex mixtures of volatile fatty acids. J Biotechnol 162:336–345.
Perez-Garcia O, Villas-Boas SG, Singhal N. 2014a. A method to calibrate metabolic network models with experimental datasets. Adv Intell Syst Comput 294:183–190.
Perez-Garcia O, Villas-Boas SG, Swift S, Chandran K, Singhal N. 2014b. Clarifying the regulation of NO/N2O production in Nitrosomonas europaea during anoxic-oxic transition via flux balance analysis of a metabolic network model. Water Res 60:267–277.
Richardson D, Felgate H, Watmough N, Thomson A, Baggs E. 2009. Mitigating release of the potent greenhouse gas N2O from the nitrogen cycle—Could enzymic regulation hold the key? Trends Biotechnol 27:388–397.
Rocha BS, Gago B, Barbosa RM, Laranjinha J. 2010. Diffusion of nitric oxide through the gastric wall upon reduction of nitrite by red wine: Physiological impact. Nitric Oxide 22:235–241.
Savinell JM, Palsson BO. 1992. Optimal selection of metabolic fluxes for in vivo measurement. I. Development of mathematical methods. J Theor Biol 155:201–214.
Schellenberger J, Que R, Fleming RMT, Thiele I, Orth JD, Feist AM, Zielinski DC, Bordbar A, Lewis NE, Rahmanian S, Kang J, Hyduke DR, Palsson BØ. 2011. Quantitative prediction of cellular metabolism with constraint-based models: The COBRA Toolbox v2.0. Nat Prot 6:1290–1307.
Schreiber F, Wunderlin P, Udert KM, Wells GF. 2012. Nitric oxide and nitrous oxide turnover in natural and engineered microbial communities: Biological pathways, chemical reactions, and novel technologies. Front Microbiol 3:372.
Schuetz R, Kuepfer L, Sauer U. 2007. Systematic evaluation of objective functions for predicting intracellular fluxes in Escherichia coli. Mol Syst Biol 3:119.
Starkenburg SR, Spieck E, Bottomley PJ. 2011. In: Ward BB, Arp DJ, Klotz MG, editors. Metabolism and genomics of nitrite oxidizing bacteria: Emphasis on studies of pure cultures and of Nitrobacter species. Washington, DC: ASM Press. p 267–2963.
Starkenburg SR, Arp DJ, Bottomley PJ. 2008a. Expression of a putative nitrite reductase and the reversible inhibition of nitrite-dependent respiration by nitric oxide in Nitrobacter winogradskyi Nb-255. Environ Microbiol 10:3036–3042.
Starkenburg SR, Larimer FW, Stein LY, Klotz MG, Chain PSG, Sayavedra-Soto LA, Poret-Peterson AT, Gentry ME, Arp DJ, Ward B, Bottomley PJ. 2008b. Complete genome sequence of Nitrobacter hamburgensis X14 and comparative genomic analysis of species within the genus Nitrobacter. Appl Environ Microbiol 74:2852–2863.
Starkenburg SR, Chain PSG, Sayavedra-Soto LA, Hauser L, Land ML, Larimer FW, Malfatti SA, Klotz MG, Bottomley PJ, Arp DJ, Hickey WJ. 2006. Genome sequence of the chemolithoautotrophic nitrite-oxidizing bacterium Nitrobacter winogradskyi Nb-255. Appl Environ Microbiol 72:2050–2063.
Stein LY. 2011. Heterotrophic nitrification and nitrifier denitrification. In: Ward BB, Arp DJ, Klotz MG, editors. Nitrification. Washington, DC: ASM Press. p 95.
Stein LY. 2010. Surveying N2O-producing pathways in bacteria. Method Enzymol 486:131–152.
Stein LY, Arp DJ, Berube PM, Chain PSG, Hauser L, Jetten MSM, Klotz MG, Larimer FW, Norton JM, Op Den Camp HJM, Shin M, Wei X. 2007. Whole-genome analysis of the ammonia-oxidizing bacterium, Nitrosomonas eutropha C91: Implications for niche adaptation. Environ Microbiol 9:2993–3007.
Stolyar S, Van Dien S, Hillesland KL, Pinel N, Lie TJ, Leigh JA, Stahl DA. 2007. Metabolic modeling of a mutualistic microbial community. Mol Syst Biol 3:92.
Taffs R, Aston JE, Brileya K, Jay Z, Klatt CG, McGlynn S, Mallette N, Montross S, Gerlach R, Inskeep WP, Ward DM, Carlson RP. 2009. In Silico approaches to study mass and energy flows in microbial consortia: A syntrophic case study. BMC Sys Biol 3:114.
Thiele I, Palsson BØ. 2010. A protocol for generating a high-quality genome-scale metabolic reconstruction. Nat Prot 5:93–121.
van den Berg RA, Hoefsloot HCJ, Westerhuis JA, Smilde AK, van der Werf MJ. 2006. Centering, scaling, and transformations: Improving the biological information content of metabolomics data. BMC Genomics 7:142.
van Loosdrecht MCM, Ekama GA, Wentzel MC, Brdjanovic D, Hooijmans CM. 2008. Modelling activated sludge processes. In: Ward BB, Arp DJ, Klotz MG, editors. Biological wastewater treatment. Principles, modelling and design. London, UK: IWA Publishing. p 361.
Varma A, Palsson BO. 1994a. Metabolic flux balancing: Basic concepts, scientific and practical use. Nat Biotechnol 12:994–998.
Varma A, Palsson BO. 1994b. Stoichiometric flux balance models quantitatively predict growth and metabolic by-product secretion in wild-type Escherichia coli W3110. Appl Environ Microbiol 60:3724–3731.
Wang JS, Hamburg SP, Pryor DE, Chandran K, Daigger GT. 2011. Emissions credits: Opportunity to promote integrated nitrogen management in the wastewater sector. Enviro Sci Technol 45:6239–6246.
Whittaker M, Bergmann D, Arciero D, Hooper AB. 2000. Electron transfer during the oxidation of ammonia by the chemolithotrophic bacterium Nitrosomonas europaea. BBA-Bioenergetics 1459:346–355.
Wuebbles DJ. 2009. Nitrous oxide: No laughing matter. Science 326(5949):57–56.
Wunderlin P, Lehmann MF, Siegrist H, Tuzson B, Joss A, Emmenegger L, Mohn J. 2013. Isotope signatures of N2O in a mixed microbial population system: Constraints on N2O producing pathways in wastewater treatment. Enviro Sci Technol 47:1339–1348.
Wunderlin P, Mohn J, Joss A, Emmenegger L, Siegrist H. 2012. Mechanisms of N2O production in biological wastewater treatment under nitrifying and denitrifying conditions. Water Res 46:1027–1037.
Yu R, Kampschreur MJ, Van Loosdrecht MCM, Chandran K. 2010. Mechanisms and specific directionality of autotrophic nitrous oxide and nitric oxide generation during transient anoxia. Enviro Sci Technol 44:1313–1319.

Supporting Information

Additional supporting information may be found in the online version of this article at the publisher's web-site.